Flow (2021), **1** E6
doi:10.1017/flo.2021.7

FLOW CAMBRIDGE UNIVERSITY PRESS

FLOW RAPID

Drop-on-demand painting of highly viscous liquids

Kyota Kamamoto[1], Hajime Onuki[1] and Yoshiyuki Tagawa[1,*]

[1]Department of Mechanical Systems Engineering, Tokyo University of Agriculture and Technology, 2-24-16 Naka-cho, Koganei, Tokyo 184-8588, Japan
*Corresponding author. E-mail: tagawayo@cc.tuat.ac.jp

Received: 22 December 2020; **Revised:** 24 June 2021; **Accepted:** 24 June 2021

Keywords: Breakup/Coalescence; Drops; Jets; Ink jets

Abstract

An on-demand painting system with a simple structure device that ejects highly viscous liquids as microjets is introduced. An impulsive motion of the container results in the ejection of a viscous liquid jet from the nozzle. This system enabled us to paint letters on a section of a car body using commercial car paint with a zero-shear viscosity of 100 Pa · s. To understand the jet velocity, we conducted systematic experiments. Experimental results showed that the jet velocity increases with the ratio between the liquid depths in the container and the nozzle, up to approximately 30 times faster than the initial velocity. However, a linear relation between the jet velocity and the ratio predicted by the previous model, which considers only the pressure impulse, does not hold for the high length ratios since the actual position of the stagnation point is different from the position predicted by the previous model. By solving the Laplace equation and using the model proposed by Gordillo *et al.* (*J. Fluid Mech.*, vol. 894, 2020, pp. A3–11), we reproduce the non-monotonic behaviour of the jet velocity as a function of the length ratio. For practical use, we improve the jet-velocity model by considering mass conservation as well as the pressure impulse.

Impact Statement

In this study, we propose a simple system to eject highly viscous liquids including non-Newtonian liquids. Although spray coating is widely used in industrial painting, such as automobile painting, it requires organic solvents to reduce the paint viscosity because the spray device can eject only low-viscosity liquids. The requirement for organic solvents is a crucial problem in terms of environmental and manufacturing costs. Our system is the solution to these problems. This system can paint letters on a section of a car body using commercial car paint (a viscous non-Newtonian fluid) without organic solvent. This result indicates that this system will contribute to the implementation of next generation printing technologies such as three-dimensional printing, printed electronics, bioprinting and needle-free injection systems. This article explains the physical mechanism of the novel drop-on-demand printing system for highly viscous liquids using the theories of fluid dynamics.

1. Introduction

Paint applied by spray coating is an important factor in determining the quality of various industrial products, such as an automobile (Toda, Salazar, & Saito, 2012). Currently, spray coating is used even though it has three major drawbacks. First, it is impossible to paint small areas because the car paint

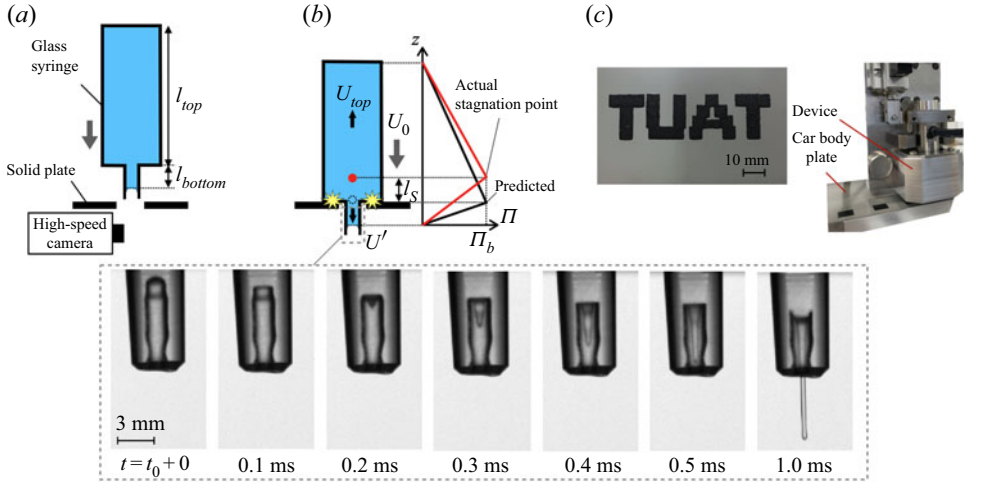

Figure 1. *(a) The device before the impact. (b) The device just right after the impact. The observation result (ν = 100 $mm^2\ s^{-1}$) (bottom) and Π - z diagram (right). (c) Result of using the new on-demand painting system (left) and the entire device (right).*

diffuses on the spray nozzle (Park & Jeon, 2018). On an automobile-coating line, the spray coating requires manual masking, which draws out the whole painting process (Kelly, 2009). Second, the paint transfer efficiency of the spray method is low at 30–70 % (Akafuah et al., 2016; Andrade, Skurtys, & Osorio, 2012; Streitberger & Dossel, 2008). Third, the spray coating requires organic solvents to reduce the paint viscosity because the spray device can eject only low-viscosity liquids. Organic solvents force the use of equipment for purification of polluted air and create a hazardous working environment for workers on the automobile-coating line. One way to avoid these problems is to eject the highly viscous liquids as a microjet on demand. This eliminates the need for organic solvents because high-viscosity paints can be ejected without dilution. In addition, masking is not required because the paint jet is narrow and can be applied to a small area. As a result, the paint transfer efficiency and working environment would be improved. Ultimately, it is expected that a painting process based on this technique will be completely automated.

Methods for ejecting highly viscous liquid microjets include laser-induced forward transfer (Koch et al., 2010; Turkoz, Kang, Deike, & Arnold, 2018), laser-induced microjet (Delrot, Modestino, Gallaire, Psaltis & Moser, 2016), microjet induced by cavitation bubbles (Gonzalez-Avila, Song, & Ohl, 2015) and acoustic printing (Foresti et al., 2018). Recently, a highly viscous liquid jet generator induced by impact was proposed (Onuki, Oi, & Tagawa, 2018). It is a simple, cheap and small system compared with the devices mentioned above. The jet velocity produced by this device can be computed with a model considering the pressure impulse approach (Antkowiak, Bremond, Le Dizès, & Villermaux, 2007; Batchelor, 1967; Cooker & Peregrine, 1995). However, in this device, the jet irregularly contacts the inner wall of the nozzle because the microjet travels a non-trivial distance inside a long nozzle, which results in nozzle clogging. Therefore, we improve the device significantly to eject highly viscous liquid microjets without clogging.

In this study, we propose a new on-demand painting device (see Figure 1*a*). The structure of the new design, in which a short nozzle is connected to a cylindrical container, is much simpler than the previous design. An impulsive motion of the container ejects a jet of highly viscous liquid. The shortness of the nozzle prevents contact between the jet and the inner wall of the nozzle.

To demonstrate the feasibility of this device, we painted letters on a section of a car body using commercial car paint with a zero-shear viscosity of 100 Pa · s and a machine employing the new device (see Figure 1*c*). Here, the commercial car paint is a shear-thinning fluid (zero-shear viscosity of

https://doi.org/10.1017/flo.2021.7 Published online by Cambridge University Press

100 Pa · s and 0.1 Pa · s at a shear rate of 100 1/s). The letters 'TUAT' were painted with more than 3600 dots automatically by a computer program. Importantly, the edges of the letters were sharply painted without using any masks, as shown in Figure 1*c*. Furthermore, no organic solvent was needed for our device. This result indicates that the new on-demand painting device can be applied to automotive painting, as well as other paintings of viscous non-Newtonian fluids.

In this letter, we investigate the jet velocity that depends on the main experimental parameters, specifically the initial liquid velocity U_0 and the ratio between liquid depth in the container and in the nozzle l_{top}/l_{bottom}, to understand the detailed mechanism of this jet ejection. In addition, we discuss a fluid dynamics model for this device.

2. Experimental Set-up and Physical Model Based on Pressure Impulse Approach

The experimental set-up is shown in Figure 1*a*. We used a glass syringe (interchangeable syringe, 10 mL, Tsubasa Industry) because it consists of a short nozzle (Luer slip tip) and a cylindrical container (barrel). The wide end of the barrel was closed with a silicon cap and a metal piece, instead of a plunger. The glass syringe was filled with silicone oil (viscosity $\nu = 1$, 10 and 100 mm^2 s^{-1}, Shin-Etsu Chemical) that fell freely and collided with a solid plate at the impact velocity U_0 (see Figure 1*b*). Immediately after the collision of the syringe, a jet emerged from the liquid–gas interface inside the nozzle with the velocity V_{jet} (see Figure 1*b*). The impact velocity U_0 was adopted as the initial velocity of the fluid. Both U_0 and V_{jet} were measured using a high-speed camera (FASTCAM SA-X, Photron) with a frame rate of 30 000 fps. The experiments were conducted in the range of $0.23 < U_0 < 1.27$ m s^{-1} and $3 < l_{top}/l_{bottom} < 95$, where l_{top} is the depth of the liquid in the container and l_{bottom} is the depth of the liquid in the nozzle (see Figure 1*a*). In this experiment, l_{top}/l_{bottom} was adjusted by fixing l_{top} to ~30 or 60 mm and changing l_{bottom} to 0.3–8.5 mm. The interface in the experiments showed complex shape with multiple undulations in some cases. However, the interface shape related to the flow focusing effect is a smooth hemisphere. Therefore, we assumed that the initial contact angle was constant in this experiment ($\theta = 25°$).

Here, we explain the physical model to predict the jet velocity of the new device based on the previous model (Onuki et al., 2018), which considered only the pressure impulse. Note that the previous model reasonably predicted the jet velocity of the previous device, which also employed impulsive motion for jet ejection. The generation process of the microjet can be divided into two regimes with different time scales: the impact interval and the focusing interval. The liquid suddenly accelerates during the impact interval, due to the impulsive force (impact duration $\leq O(10^{-4})$s). After the impact interval (focusing duration $\gg O(10^{-4})$s), the microjet emerges through a flow-focusing effect during the focusing interval.

During the impact interval, a sudden change in the motion of the container produces large pressure gradients in the fluid, which in turn produces a sudden change in the liquid velocity (Batchelor, 1967). Considering the short-time dynamics due to the impact, and assuming that the device moves only in the vertical direction z, the dynamics of the liquid is governed by $\partial \boldsymbol{u}/\partial t = -(1/\rho)(\partial p/\partial z)$, where $\boldsymbol{u}$ is the liquid velocity, ρ is the density and p is the pressure. When the liquid is accelerated in a static state to the velocity U due to the impact, the liquid velocity right after the impact is derived as $U = -(1/\rho)(\partial \Pi/\partial z)$, where Π is the pressure impulse, or the time integration of the pressure during the impact period $\tau(\Pi = \int_0^\tau p\,\mathrm{d}t)$. The liquid velocity U is proportional to the gradient of pressure impulse $\partial \Pi/\partial z$. In the new device, the associated impulse pressure satisfies $p = p_a$, where p_a is the atmospheric pressure, at the gas–liquid interface inside the nozzle and at the top of the container. Thus, the pressure impulse distribution can be sketched as shown by the black line in Figure 1*b*. The stagnation point is at the base of the nozzle shown as a dotted circle in Figure 1*b*. The gradient of the pressure impulse inside the nozzle $(\partial \Pi/\partial z)_{bottom}$ is calculated with a geometrical relation as $(\partial \Pi/\partial z)_{bottom} = l_{top}/l_{bottom}(\partial \Pi/\partial z)_{top}$, where $(\partial \Pi/\partial z)_{top}$ is the gradient of the pressure impulse inside the container. Thus, the liquid velocity inside the nozzle U' during the impact interval can be described as $U' = (l_{top}/l_{bottom})U_{top}$, where U_{top} indicates the liquid velocity in the container, which is approximated to the velocity at the bottom of the container U_0.

https://doi.org/10.1017/flo.2021.7 Published online by Cambridge University Press

During the focusing interval, previous research (Kiyama, Tagawa, Ando, & Kameda, 2016; Peters et al., 2013; Tagawa et al., 2012) has revealed that the jet velocity V_{jet} induced by the flow-focusing effect is proportional to the liquid velocity inside the nozzle U'. Thus, the jet velocity ratio V_{jet}/U_0 in our device is estimated as

$$\frac{V_{jet}}{U_0} = \beta \frac{l_{top}}{l_{bottom}}, \tag{1}$$

where β, defined as the increment ratio of the jet velocity, is a coefficient related to the liquid viscosity and the flow-focusing effect determined by the initial shape of the interface (i.e. contact angle θ). This physical model, (1), predicts a linear relation between the jet velocity ratio V_{jet}/U_0 and the length ratio l_{top}/l_{bottom}.

3. Results and Discussion

Figure 2*a* shows the measured velocity ratios V_{jet}/U_0 for three kinematic viscosities (1, 10 and 100 mm^2 s^{-1}), which monotonically increased with the length ratio l_{top}/l_{bottom}. The jet generated from the new device was accelerated by more than 10 times at approximately $l_{top}/l_{bottom} = 15$ for 1 and 10 mm^2 s^{-1}. Especially, the jet velocity V_{jet} of the 1 mm^2 s^{-1} liquid was more than 30 times faster than the initial velocity U_0, although the rate of velocity increase became smaller for $l_{top}/l_{bottom} > 40$. In contrast, the velocity ratio in the case of high viscosity (100 mm^2 s^{-1}) continued to increase even when $l_{top}/l_{bottom} > 40$. This indicated that the new device using impact with a short nozzle is suitable for ejection of highly viscous liquids because highly viscous liquids can be accelerated efficiently.

When the length ratio was small ($l_{top}/l_{bottom} < 15$), the experimental data agreed well with (1), which predicts a linear increase relation. However, when the length ratio was large ($l_{top}/l_{bottom} > 40$), the velocity ratios V_{jet}/U_0 of all liquids increased nonlinearly and deviated significantly from the linear model (see Figure 2*a*). Hence, the model considering only the pressure impulse, as in the previous research, cannot accurately describe the jet velocity for the whole range of length ratios.

To examine the reason for the deviation between the experimental data and (1), we analysed the flow field during the impact interval. We considered the potential flow while neglecting the effect of the surface tension and the viscosity. Applying the nabla operator to the velocity $\boldsymbol{U}$ yields $\boldsymbol{\nabla U} = \nabla^2\phi = 0$, where $\phi = -\Pi/\rho$. We solved this Laplace equation by numerical means using commercial software (COMSOL Multiphysics). The boundary conditions are shown in Figure 2*b*. In the numerical calculation, a triangle mesh was used, the maximum size of which was 0.1 mm under conditions of two-dimensional axisymmetry.

The calculated streamlines of the potential flow field and the magnitude of the velocity inside the new device are shown in Figure 2*c*. Remarkably, the position of the actual stagnation point was significantly higher than the position predicted by (1). We further analyse this flow in the next section.

4. Potential Flow Analysis and Renewed Jet Velocity Model

The solution of the Laplace equation can be used to understand the nonlinear trend of the jet velocity as a function of the length ratio l_{top}/l_{bottom}, especially for the low-viscosity liquid in experiments. Here we solve the Laplace equation in various conditions and use the model proposed by Gordillo, Onuki, and Tagawa (2020) for predicting the jet velocity affected by the flow focusing effect at the curved interface. Note that the initial liquid velocity imposed upstream of the curved surface should be given to use the results of Gordillo et al. (2020). Thus we first calculate the initial velocity, V, by solving the Laplace equation numerically and then substitute V into the model proposed by Gordillo et al. (2020).

The detailed procedure is as follows: In order to obtain the initial liquid velocity upstream of the curved meniscus in the nozzle, the interface shape was set as a flat shape. We set $l_{top} = 30$ mm, $l_{bottom} = 0.30, 0.43, 0.60, 1.0, 5.0, 9.0$ mm, $r = 0.6$ mm, $R = 6.2$ mm, similar to experimental values. Under each condition, the Laplace equation was solved to obtain the initial liquid velocity V.

https://doi.org/10.1017/flo.2021.7 Published online by Cambridge University Press

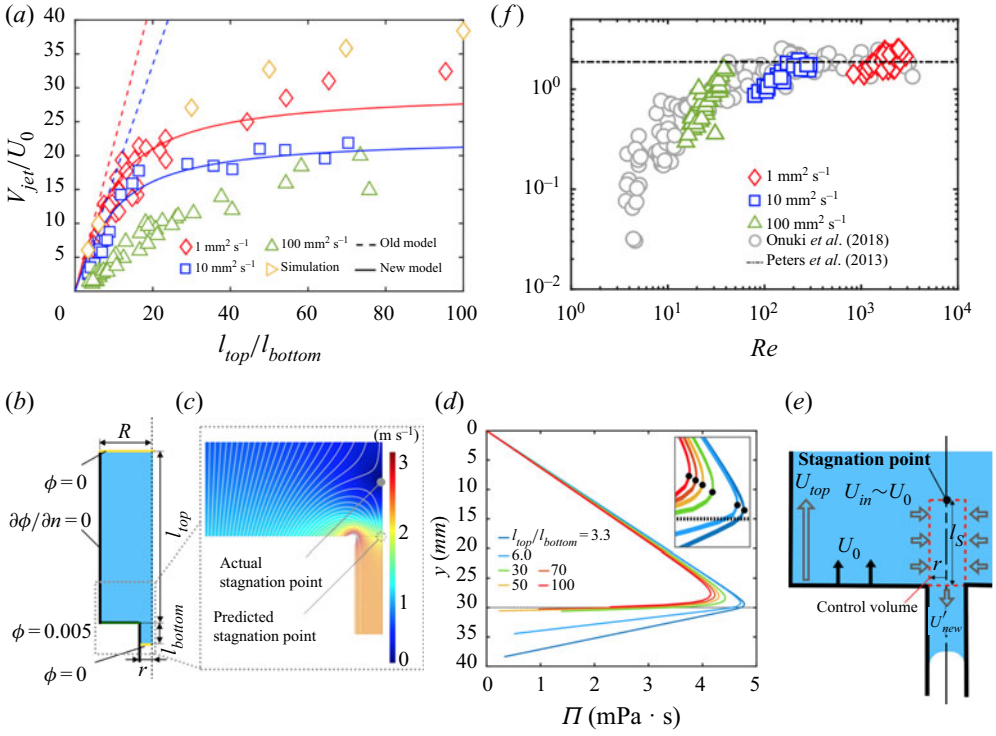

Figure 2. *(a) Relation between the velocity ratio V_{jet}/U_0 and the length ratio l_{top}/l_{bottom}. (b) Geometry for the numerical set-up. (c) Velocity fields and streamline immediately after the impact. (d) Pressure impulse distribution along the vertical axis. The position of the stagnation point is shown as a black dot while the predicted stagnation point is indicated by the dotted line. (e) Liquid near the edge of the nozzle. (f) Increment ratio of jet velocity β as a function of Reynolds number Re.*

By substituting the initial velocity V and initial contact angle $\theta = 25°$ into the following equation proposed by Gordillo et al. (2020), the jet velocity V_{jet} is

$$V_{jet} = V v_{n0} \left(\frac{k^2}{3 + k^2} \right)^{-2/3}, \tag{2}$$

where $v_{n0} = 0.31 \cos\theta + 0.90 \fallingdotseq 1.2$ and $k^2 = 1.60/\cos\theta + 0.33 \fallingdotseq 2.1$ in this calculation.

Figure 2*a* shows the jet velocity predicted by solving the Laplace equation and using the model of Gordillo et al. (2020). The jet velocity increased non-monotonically with increasing the length ratio l_{top}/l_{bottom}. This trend was quite consistent with the jet velocity measured in experiments. The quantitative agreement between the jet velocities by the calculation and those in the experiment was achieved for lower length ratio l_{top}/l_{bottom}, while the simulated result was slightly larger than the experimental one when the length ratio l_{top}/l_{bottom} was large. A possible reason is the viscous drag in the experiments.

To further understand this nonlinear trend of the jet velocity, we plot the pressure impulse distribution along the vertical axis of the device in Figure 2*d*. The position of the stagnation point indicated by the black marker in the inset of Figure 2*d* was significantly different from the predicted position denoted by the dashed line for larger length ratio l_{top}/l_{bottom}. Furthermore, the pressure impulse at the stagnation point slightly decreased as the length ratio l_{top}/l_{bottom} increased. This is why the predicted jet velocities by the previous model (Onuki et al., 2018) deviated from the experimental results for large length ratio l_{top}/l_{bottom}.

https://doi.org/10.1017/flo.2021.7 Published online by Cambridge University Press

For the physical interpretation, solving the Laplace equation and using the model of Gordillo et al. (2020) may be good enough. Nevertheless, we believe that a simple model which explicitly includes the lengths, l_{top}, l_{bottom} and r, is quite useful for designing such jetting devices. Therefore we revise the pressure impulse model of Onuki et al. (2018) as described below.

The actual pressure impulse distribution can be illustrated as the red solid line in Figure 1*b*. The distance between the actual stagnation point and the predicted stagnation point is denoted as l_s. The gradient of the pressure impulse considering the distance l_s is described as $(\partial \Pi/\partial z)_{bottom^*} = (l_{top} - l_s)/(l_{bottom} + l_s)(\partial \Pi/\partial z)_{top^*}$, where $(\partial \Pi/\partial z)_{bottom^*}$ and $(\partial \Pi/\partial z)_{top^*}$ are the actual gradients of the pressure impulse under and above the stagnation point, respectively. Thus, the liquid velocity under the actual stagnation point U'_{new} is

$$U'_{new} = \frac{l_{top} - l_s}{l_{bottom} + l_s} U_0. \tag{3}$$

To predict the distance l_s, we consider the mass conservation of the liquid near the nozzle. The control volume is indicated by a red dashed rectangle in Figure 2*e*. Assuming that the inlet mass flow comes through the side of the control volume with velocity $U_{in} \sim U_0$ and the outlet mass flow goes through the bottom of the control volume with the velocity U'_{new}, we obtain $\pi r^2 U'_{new} = 2\pi r l_s U_0$, where r is the radius of the nozzle (see Figure 2*e*). Thus, the new jet velocity model is

$$\frac{V_{jet\_new}}{U_0} = \beta \frac{-(2l_{bottom} + r) + \sqrt{(2l_{bottom} + r)^2 + 8rl_{top}}}{2r}. \tag{4}$$

The velocity ratio is affected greatly by the absolute values of l_{top}, l_{bottom} and r.

To validate the new model, the new models for 1 mm^2 s^{-1} and 10 mm^2 s^{-1} are shown in Figure 2*a* as red and blue solid curves, respectively. The two solid curves are drawn with changing l_{bottom} and with fixed $l_{top} = 60$ mm, $U_0 = 1.0$ m s^{-1}, $r = 0.6$ mm, $\beta = 2.17$ (red) and $\beta = 1.67$ (blue). The new model, (4), shows a nonlinear trend, similar to the experimental results, which cannot be described with the previous linear model, (1). For further validation, we focused on the relation between the increment ratio β and Reynolds number $Re(= U'_{new} r/\nu)$, as previous research found that β is a function of Re because β is affected by viscous drag during the focusing interval. Figure 2*e* shows that the results of the previous research and current research are in good agreement, which indicates that the new model successfully predicts U'_{new}.

5. Conclusion

We propose a new device to solve a problem in previous research for a highly viscous on-demand printing technology. The new device ejects highly viscous liquid, such as commercial car paint with a zero-shear viscosity of 100 Pa · s. The jet velocity was increased by approximately up to 30 times the impact velocity. The experimental results showed that the linear model, (1), which considers only the pressure impulse, cannot describe the nonlinear behaviour of the jet velocity as a function of the length ratio l_{top}/l_{bottom}. To explore the reason for this, we solved the Laplace equation by numerical means and found that the position of the stagnation point of the flow inside the container is significantly higher than that assumed by the linear model, (1). Here we solve the Laplace equation for obtaining the initial velocity imposed upstream of the curved surface and use the flow focusing model proposed by Gordillo et al. (2020). Remarkably the nonlinear behaviour of the jet against the length ratio l_{top}/l_{bottom} is successfully reproduced. Furthermore, to obtain technologically useful information, we revise the previous model (Onuki et al., 2018) by considering mass conservation as well as the pressure impulse. The new model closely describes the nonlinear behaviour of the jet velocity. These results indicate that the device we developed can be applied to a drop-on-demand painting system with highly viscous liquids, such as automobile painting.

https://doi.org/10.1017/flo.2021.7 Published online by Cambridge University Press

Acknowledgements. We thank Y. Nishi for applying automotive paint to the car body panels.

Funding Statement. This work was supported by the Japan Society for the Promotion of Science, KAKENHI Grant Nos 17H01246 and 20H00223, and Adaptable and Seamless Technology transfer Program through Target-driven R&D (A-STEP) from Japan Science and Technology Agency (JST).

Declaration of Interests. The authors report no conflict of interest.

Author Contributions. Conceptualization, Y.T.; methodology, K.K. and H.O.; data curation, K.K.; data visualisation, K.K.; writing original draft, K.K. and Y.T. All authors approved the final submitted draft.

Data Availability Statement. The data that support the findings of this study are available within the article.

Ethical Standards. The research meets all ethical guidelines, including adherence to the legal requirements of the study country.

References

Akafuah, N. K., Poozesh, S., Salaimeh, A., Patrick, G., Lawler, K., & Saito, K. (2016). Evolution of the automotive body coating process–a review. *Coatings*, *6*(2), 24.

Andrade, R. D., Skurtys, O., & Osorio, F. A. (2012). Atomizing spray systems for application of edible coatings. *Comprehensive Reviews in Food Science and Food Safety*, *11*(3), 323–337.

Antkowiak, A., Bremond, N., Le Dizès, S., & Villermaux, E. (2007). Short-term dynamics of a density interface following an impact. *Journal of Fluid Mechanics*, *577*, 241–250.

Batchelor, G. K. (1967). *An introduction to fluid dynamics*, pp. 471–474. Cambridge University Press.

Cooker, M. J., & Peregrine, D. (1995). Pressure-impulse theory for liquid impact problems. *Journal of Fluid Mechanics*, *297*, 193–214.

Delrot, P., Modestino, M. A., Gallaire, F., Psaltis, D., & Moser, C. (2016). Inkjet printing of viscous monodisperse microdroplets by laser-induced flow focusing. *Physical Review Applied*, *6*(2), 024003.

Foresti, D., Kroll, K. T., Amissah, R., Sillani, F., Homan, K. A., Poulikakos, D., & Lewis, J. A. (2018). Acoustophoretic printing. *Science Advances*, *4*(8), eaat1659.

Gonzalez-Avila, S. R., Song, C., & Ohl, C.-D. (2015). Fast transient microjets induced by hemispherical cavitation bubbles. *Journal of Fluid Mechanics*, *767*, 31–51.

Gordillo, J. M., Onuki, H., & Tagawa, Y. (2020). Impulsive generation of jets by flow focusing. *Journal of Fluid Mechanics*, *894*, A3–11.

Kelly, C. (2009). *Automotive paint technology into the 21st century*, p. 49. Report by International Specialised Skills Institute Inc., Melbourne Australian Government.

Kiyama, A., Tagawa, Y., Ando, K., & Kameda, M. (2016). Effects of a water hammer and cavitation on jet formation in a test tube. *Journal of Fluid Mechanics*, *787*, 224–236.

Koch, L., Kuhn, S., Sorg, H., Gruene, M., Schlie, S., Gaebel, R., . . . Chichkov, B. (2010). Laser printing of skin cells and human stem cells. *Tissue Engineering Part C: Methods*, *16*(5), 847–854.

Onuki, H., Oi, Y., & Tagawa, Y. (2018). Microjet generator for highly viscous fluids. *Physical Review Applied*, *9*(1), 014035.

Park, K., & Jeon, D. (2018). Optimization of tool path pitch of spray painting robots for automotive painting quality. *International Journal of Control, Automation and Systems*, *16*(6), 2832–2838.

Peters, I. R., Tagawa, Y., Oudalov, N., Sun, C., Prosperetti, A., Lohse, D., & van der Meer, D. (2013). Highly focused supersonic microjets: Numerical simulations. *Journal of Fluid Mechanics*, *719*, 587–605.

Streitberger, H.-J., & Dossel, K.-F. (2008). *Automotive paints and coatings*, pp. 259–303. John Wiley & Sons.

Tagawa, Y., Oudalov, N., Visser, C. W., Peters, I. R., van der Meer, D., Sun, C., Prosperetti, A., & Lohse, D. (2012). Highly focused supersonic microjets. *Physical Review X*, *2*(3), 031002.

Toda, K., Salazar, A., & Saito, K. (2012). *Automotive painting technology: A Monozukuri-Hitozukuri perspective*, pp. 5–43. Springer.

Turkoz, E., Kang, S., Deike, L., & Arnold, C. B. (2018). Subthreshold laser jetting via flow-focusing in laser-induced forward transfer. *Physical Review Fluids*, *3*(8), 082201.

Cite this article: Kamamoto, K., Onuki, H., & Tagawa, Y. (2021). Drop-on-demand painting of highly viscous liquids. *Flow*, *1*, E6. doi:10.1017/flo.2021.7